Journal of the European Ceramic Society 38 (2018) 4476–4482

Contents lists available at ScienceDirect

Journal of the European Ceramic Society

journal homepage: www.elsevier.com/locate/jeurceramsoc

Original Article

Dielectric breakdown toughness from filament induced dielectric breakdown in borosilicate glass

Pia-Kristina Fischer, Gerold A. Schneider*

Institute of Advanced Ceramics, Hamburg University of Technology, Denickestraße 15, 21073, Hamburg, Germany

ARTICLE INFO

Keywords:
Dielectric breakdown
Dielectric breakdown strength
Dielectric breakdown toughness
Energy release rate
Conductive filament

ABSTRACT

The dielectric breakdown strength of borosilicate glass was measured as a function of the length of a conducting filament in order to determine the critical energy release for the growth of a breakdown channel. The concept is similar to the experimental determination of the toughness in fracture mechanics and based on a Griffith type model for the electrical energy release rate in dielectric materials with space charge limited conductivity. By Focused-Ion-Beam-milling and Pt-deposition, up to 100 μm long conductive channels were fabricated in 163 μm thick borosilicate glass substrates. The dielectric breakdown strength of substrates with filaments longer than 30 μm could be very well described by a $\frac{1}{\sqrt{filament\ length}}$ -dependence predicted by the model Schneider, 2013. With these results for the first time a critical energy release rate for dielectric breakdown was determined being 6.30 ± 0.95 mJ/m.

1. Introduction

Even though dielectric breakdown is a limiting factor for the reliability of electronic devices and components [2,3,4] and despite almost 100 years of research there is no commonly accepted understanding of this phenomenon. There is a great deal of effort being made to improve electrical performance in semiconductor electronics and batteries, but only a few research groups are concerned with the mechanism of dielectric breakdown itself. It seems to be clear that like for the mechanical strength and reliability it has to be distinguished between intrinsic and extrinsic failure mechanism [5]. Applying density function perturbation theory calculations (DFPT) it was shown that von Hippels avalanche model is able to predict the intrinsic breakdown for covalently bonded and ionic materials [6]. For the extrinsic breakdown the existing experimental results are more controversial. In this investigation we favour theoretical models based on the idea of a filamentary breakdown [1,5,7]. In such a model small conducting filaments of length a underneath the electrode in an electrical insulator of thickness d and a dielectric constant ε are assumed. These might be grain boundaries, chemical inhomogeneities with locally increased conductivities or injected charges. Under the application of the external homogeneous electric field E these tiny filaments lead to an electric field enhancement at the filament tip – similar to the mechanical stress field singularity in fracture mechanics, which triggers the dielectric breakdown (Fig. 1). In analogy to fracture mechanics it could be shown that this concept enables the formulation of an energy release rate G_{bd}, which is the released electric field energy per filament extension [1].

$$G_{bd} = \frac{\pi}{8}\varepsilon\varepsilon_0 a d E^2 \tag{1}$$

ε_0 is the permittivity of free space. Dielectric breakdown occurs, when the energy release rate reaches a critical value which is G_c.

$$G_{bd} = G_c \tag{2}$$

Eq. (2) can be solved for the corresponding applied electric field at dielectric breakdown E_{bd} [1]:

$$E_{bd} = \frac{1}{c}\sqrt{\frac{6}{5\pi}}\sqrt{\frac{G_c}{\varepsilon\varepsilon_0}}\frac{1}{\sqrt{d}}\frac{1}{\sqrt{a}} \tag{3}$$

with c ≅ $\sqrt{0.15}$. It has been shown in several publications that the extrinsic breakdown strength E_{bd} is proportional to $1/\sqrt{d}$ [5,8,9,10]. In addition, more recently it was shown that also the proportionality to $1/\sqrt{\varepsilon}$ holds for bulk ceramics and polymers [11]. These experimental results support the physical concept of this breakdown model.

Although the temperature dependent breakdown data from Hoshina et al. [12] up to 100 °C are best fitted by the Griffith-type energy release rate model when compared to an intrinsic and thermal breakdown model. A necessity for the result given in Eq. (1) is, that space charge limited conduction (SCLC) prevails in the electrically insulating material [11,13]. This could be shown for several ceramics and is a decisive difference to other breakdown models [11,14].

In this investigation we apply this theoretical concept to determine

* Corresponding author.
E-mail address: g.schneider@tuhh.de (G.A. Schneider).

https://doi.org/10.1016/j.jeurceramsoc.2018.05.036
Received 26 April 2018; Received in revised form 25 May 2018; Accepted 27 May 2018
Available online 28 May 2018

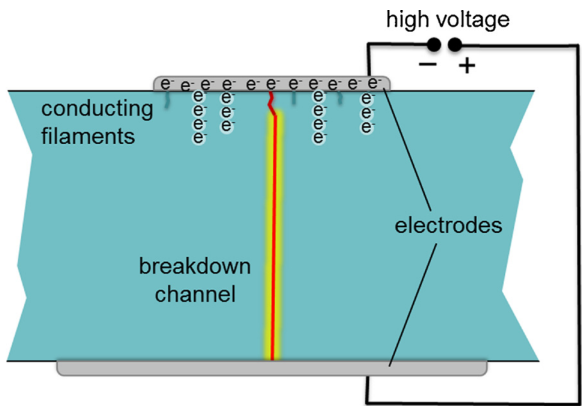

Fig. 1. Schematic illustration of the dielectric breakdown initiated by conducting filaments.

the dielectric breakdown energy release rate G_c experimentally introducing well-defined artificial conducting channels of length a and radius of curvature r_0 at the filament tip.

2. Material and methods

2.1. Material

To our knowledge there are no dielectric breakdown studies with artificially prepared conducting filaments similar to fracture toughness measurements with artificially introduced and sharpened notches [15,16,17]. Consequently the critical length of a filament as a function of the applied electric field is not known yet. The only hint we could use was our own publication [5] where we used the transition between extrinsic and intrinsic dielectric breakdown strength to estimate the size of the natural filaments of the order of some microns for ceramics. In order to avoid as much as possible natural defects such as cracks or grain boundaries as well as anisotropic material properties an amorphous glass was chosen as model material. The reason we did not use single crystals as in previous experiments [5,18] is related to the fact that we observed preferential breakdown channel directions in the single crystals along certain crystal directions.

Commercially available borosilicate cover glasses were used. A summary of the physical characteristics can be found in Table 1.

Before every measurement the samples were cleaned with ethanol and dried at 60 °C for half an hour. For conduction measurements until breakdown and breakdown tests, in addition, electrodes with conductive silver paint were applied, which is described in the following section in more detail.

2.2. Conductivity measurements

Electrical conductivity measurements were performed to determine

Table 1
Main characteristics of the used cover glass (No.1, LabSolute, Germany) at T = 293 K [19].

Material	Borosilicate glass 3.3, Th. Geyer
Composition	80.6 % SiO2, 13.0 % B2O3, 4.0 % Na2O & K2O, 2.4 % Al2O3
Nominal thickness	163 ± 7 µm*
Dimension	24 × 32 mm
Density	2.23 g/cm³
Permittivity	4*
Loss factor tan δ	0.016*
Thermal conductivity	1.2 W·m-1·K-1
Young modulus	64 GPa

* own measurement.

whether the dielectric breakdown takes place in the space charge limited conduction (SCLC) regime. To cover a wide voltage range the conductivity measurements were divided in two parts. Conduction measurements up to 1 kV were performed in air with a more sensitive device and high voltage conduction measurements until dielectric breakdown were conducted in silicon oil to avoid partial discharge and flash over. All measurements were carried out at room temperature.

2.2.1. Conductivity measurements up to 1 kV

For these measurements a high-voltage meter Agilent 4339B was used. It can provide dc voltages up to 1 kV and detects currents from 60 fA to 500 µA. The measurement setup, consisting of three electrodes, is placed in a shielded resistivity cell (Agilent 16008B). With these three electrodes, namely a high-voltage (HV)-electrode with 18 mm and a ring-electrode with 22 mm diameter on same potential and the measuring-electrode with a dimension of 110 × 110 mm on opposite potential, the volume current through the sample was detected. With the ring electrode it is ensured that no surface current is detected. The voltage was applied stepwise to the samples and kept constant for 120 s, meanwhile the current was detected every 400 ms. From 1 V to 10 V the voltage was increased in 5 V-steps, from 10 V to 100 V in 10 V-steps and 100 V to 1 kV in 100 V-steps. For each voltage level, the mean current was determined from the last two-thirds of the values recorded during the measurement as done in previous work by Neusel [11].

2.2.2. Conductivity measurements until dielectric breakdown

For the conduction measurement until breakdown a combined setup consisting of high-voltage generator and a picoampere meter was used. The high-voltage generator with voltages up 70 kV ER75P4 (Glassman high voltage, Inc., UK) was linked up with a picoampere meter M1501 P (Sefelec S.A.S., France), which can detect currents from 200 pA to 2 µA. Conductive silver paint was used to provide good electric contact between the high voltage source and the substrate. The applied electrodes had different sizes to minimize field enhancements at the edges. The electrode on the ground side had a radius of $R_1 = 5$ mm and the electrode, which was connected to the positive high voltage, had a radius of $R_2 = 9$ mm (see Fig. 2b). They were dried at 60 °C for 1 h to evaporate the solvent. For the measurement the samples were clamped between a steel-made Rogowski-like profile and a brass-made pin-electrode (see Fig. 2a).

The voltage was increased in 1 kV-steps and after a stabilization time of 20 s kept constant for 5 s for the current detection. The current signal was detected every 150 ms and as for the 1 kV conductivity measurements, the mean current for each voltage level was calculated from the last two-thirds of the collected data points. The voltage was raised until it collapsed and the device changed to the current controlled mode with a current of 2 µA, indicating dielectric breakdown.

2.3. FIB-preparation

Conductive filaments of certain depth into the glass substrates were introduced using a Focused Ion Beam (FIB) instrument (FEI FIB Strata 205 single beam). It is equipped with a gallium liquid metal ion source (Ga-LMIS) for imaging and sample modification via material deposition. With two different gas injection systems (GIS) the deposition of a conductor (Pt) and an insulator (SiO_2) is possible. The acceleration voltage for the Ga^+-ions can be adjusted between 5 and 30 kV and the ion beam current can be set stepwise between 1 pA up to 20 nA maximum. The highest possible spatial resolution is approx. 7 nm. Before the samples could be inserted into the vacuum chamber of the FIB, they were cleaned with ethanol and the surface was sputtered with gold to obviate charging effects. Per sample one defined channel was milled in the middle of the rectangular substrate. For the different sized channels, pre-experiments had been conducted to determine the parameters to obtain filaments in the desired depth and shape. For this purpose, a certain circular area and depth were set in the program of the FIB and

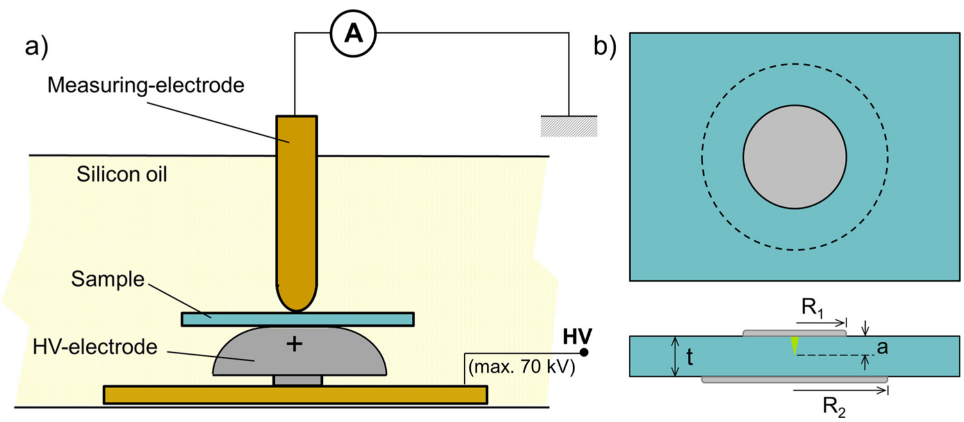

Fig. 2. Schematic image of a) the measurement setup for the conduction measurement until dielectric breakdown. The bottom electrode was connected to the positive HV-source and shaped similar to a Rogowski-profile. In contrast, the counter electrode was a brass pin, connected to the picoampere meter and functioning as ground. In b) a schematic image of the prepared sample with its silver paint electrodes is shown.

Table 2
Overview of the prepared samples with conductive filaments. The inaccuracy of the geometrical measurements is less than 5%.

Filament length a (μm)	10	20	30	40	50	60	70	80	100
Milling depth z (μm)	8	14,9	22,5	30	35	45	52,5	60	73
Radius of milling area r_a (μm)	0,8	1,5	2,25	3,0	3,5	4,5	5,25	6,0	7,3
Beam current (pA)	30	300	500	1000	1000	3000	3000	3000	5000
Number of samples n	2 (+1)	3	3 (+3)	3	7	3	2	3	2

after the milling was finished the created channel was gauged. To determine the geometry of the milled channel, part of the sample had to be milled out additionally. Tilting the sample holder enabled to image the cross section of the filament. The filament's geometry was gauged including the angle of inclination. This procedure was repeated for the different channel depths shown in Fig. 4, and thus a calibration equation was obtained. The obtained channels were always a factor 1.35 longer than the set milling depth. During the milling of the filaments, Pt had to be vapor-deposited on the entire visible surface from time to time. Due to the single beam, Ga^{+}-ions, which are also used for imaging, slowly removed the originally deposited 5 nm thin gold layer, whenever an image was scanned. This Pt-deposition is only a few nanometers thick and has no effect on the milling of the filament. After the filaments were milled according to the parameters given in Table 2, the hollow channel was carefully filled with Pt to ensure a conductive filament without any cavities.

Table 2 summarizes the prepared channels displayed. The numbers in brackets are samples with additionally sharpened filaments. This means that after the filaments were milled, an extra fine tip was added to the first root tip applying the lowest ion beam current of 1 pA and the smallest point area with a radius of r_a = 50 nm as shown in Fig. 3. These samples were prepared to check if the root tip is sharp enough as its radius of curvature has a huge impact on the electric field distribution at the tip.

Subsequent to the FIB-preparation for protection a droplet of silver paint was deposited above the filament. After drying for at least 30 min at 60 °C the gold layer was removed from the sample and the electrodes were applied out of conductive silver paint.

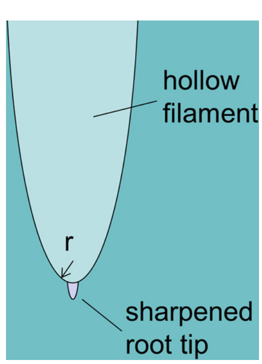

Fig. 3. Illustration of the sharpened root tip.

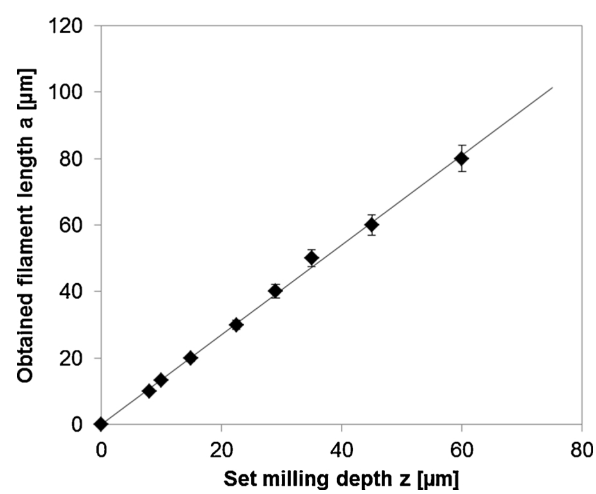

Fig. 4. Obtained filament length *a* versus the set milling depth *z* of the control unit of the FIB. The statistical analysis of the data leads to: $a = 1.35\ z$.

2.4. Dielectric breakdown test

For the breakdown tests the same high voltage source and electrode setup as for the conductivity measurements until breakdown was used but without the picoampere meter.

When measuring the FIB-prepared samples the conductive filaments were always placed on the negative or ground pole side, respectively, except from three samples with 50 μm filaments. These were placed reversed so that the filament faced the positive pole to examine whether electrons or holes are injected. The voltage was increased with a ramp of 0.2 kV/s until breakdown occurred. Breakdown was detected when the voltage signal suddenly dropped and a current flow arose. Experimentally, dielectric breakdown is detected when the Sefelec device detects a current flow and no steady voltage can be further build up any more. The current flow is limited to 2 μA due to an inner current

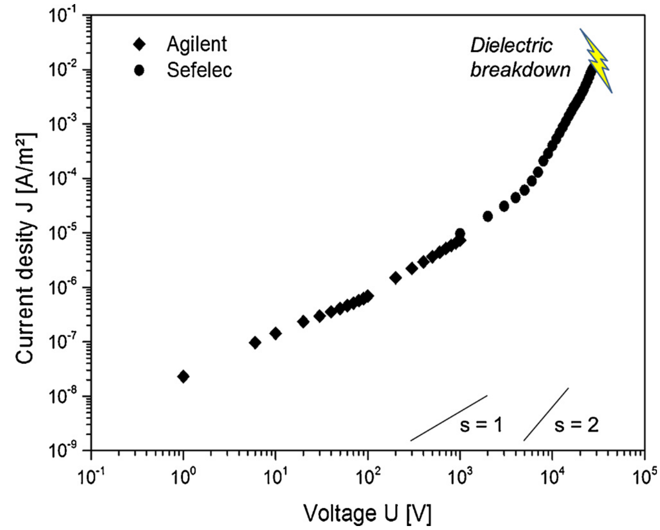

Fig. 5. Typical current density versus voltage curve of the investigated 163 µm thick glass. The values from 1 V to 1000 V were measured with the Agilent device. Beyond that voltage the Sefelec device was used until dielectric breakdown occurred. The transition voltage U_{tr} between the ohmic (s = 1) and space charge limited (s≃2) conduction regime is shown to be around 3–5 kV. The indication of the standard deviation was omitted, since it was quite small and barely visible at the logarithmic scale.

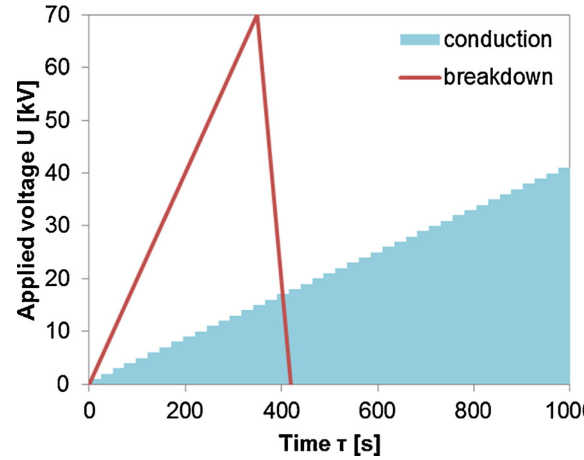

Fig. 6. Comparison of the applied voltage during breakdown measurements and conduction measurements. For the pure breakdown measurements the voltage was increased with a ramp of 0.2 kV/s and for the conduction measurements the voltage was increased stepwise by 1 kV and kept constant for 20 s stabilization time plus 5 s for the current detection, corresponding to an average ramp of 40 V/s.

limitation of the device. The dielectric breakdown event was always accompanied by noise emission and a breakdown channel. The dielectric breakdown voltage was defined as the maximum voltage right before the voltage collapse and the detection of a breakdown channel. As the voltage was detected with a rate of 250 ms the precision of the breakdown voltage is typically ± 50 V.

3. Results

3.1. Conductivity measurements

In Fig. 5, the measured current density J is plotted as a function of the applied voltage U. The diagram includes the values of the low-voltage measurement from 1 to 1000 V and the high-voltage measurements from 1000 V until breakdown. The shown curve is the mean of four measurements on different glass samples. The slight step at 1 kV is due to the change of the equipment and is within the normal scatter of the data. Therefore, it can be assumed that even without ring electrode no or only very small surface currents were measured. In the lower voltage range, the measured data points describe a slope s of approximately 1, which indicates ohmic conductivity in a double logarithmic plot. Beyond voltages of 2 kV, the rise of the current density increases and reaches a slope s of ≥ 2, indicating SCLC. The transition from ohmic to space charge limited conduction is quite sharp and the transition voltage U_{tr} is around 3–5 kV. This behavior was already found for Al_2O_3 by Talbi et al. [14] and confirmed for TiO_2, $BaTiO_3$, ZrO_2 and AlN by Neusel and Schneider [11].

The conduction measurements were performed with an average voltage ramp of 40 V/s which is 5 times slower than the ramp of 200 V/s for the breakdown experiments (see Fig. 6). The time to dielectric breakdown increases from approx. 240 s to 700 s. The dielectric breakdown at the end of the conduction measurements occurred on average at 28.0 ± 1.2 kV, which is significantly lower than the breakdown strength of 47.7 ± 4.7 kV during breakdown measurements. This time or ramp dependence of the dielectric breakdown strength is well known, but it was not possible to have the same ramp here as in the breakdown measurements since the conduction measurement needs time for current stabilization. As for the breakdown experiments with the 200 V/s ramp, a single breakdown channel can be seen after the conduction measurement until breakdown.

3.2. FIB-milled filaments

Because the sample must be destroyed to measure the geometry of the channel as described in Section 2.3, only channels used for the calibration can be seen here, not the actually conductive filaments, which were prepared for the breakdown measurements. Due to the standardized FIBing process, the images shown here can be considered to be representative for all samples. The FIB-milled filaments show a conical shape with a sharp pointed tip (Fig. 7). For all the calibration filaments with their different length varying between 10–80 µm the same ratio Ψ between diameter D and length a of 0.15 was measured and a root tip radius r of ~500 nm. The filaments have a smooth surface and are homogeneously filled with platinum.

As known from fracture mechanics, the root tip radius has a big influence on the stress distribution and thereby on the fracture toughness. It is also known that there is a “critical notch root radius” for fracture tests and if this radius is exceeded, the calculated fracture toughness could be overestimated [20]. Also in electric fields, sharp edges are crucial. Therefore, a comparison of different root tip radii was made in addition. In Fig. 8 an example of a filament with a sharpened root tip is provided. The radius of curvature at this tiny extra tip is around 50 nm.

3.3. Dielectric breakdown tests

Fig. 9 shows the results of the breakdown tests of the sound (without artificial conducting filament) and the FIB-prepared glass substrates. The breakdown strength E_{bd}, defined as breakdown voltage per sample thickness, is plotted as a function of filament length a. All samples showed a single breakdown channel within the area of the electrodes. Samples where the breakdown occurred at the electrode edges were not included, because of the field enhancements at the electrode edges. As dashed line the prediction of the Griffith type energy release rate model is included. The sound breakdown strength is 292.87 ± 28.88 kV/mm, which is a scatter of about 10% standard deviation. Samples with 10 and 20 µm deep filaments were produced and tested as well, but these channels did not initiate breakdown, so the measured values were also counted as sound samples. In order to visualize these tests in Fig. 9 they are included with white rhombs. In samples with filaments equal to 30 µm length or longer, the breakdown was initiated at these FIB-

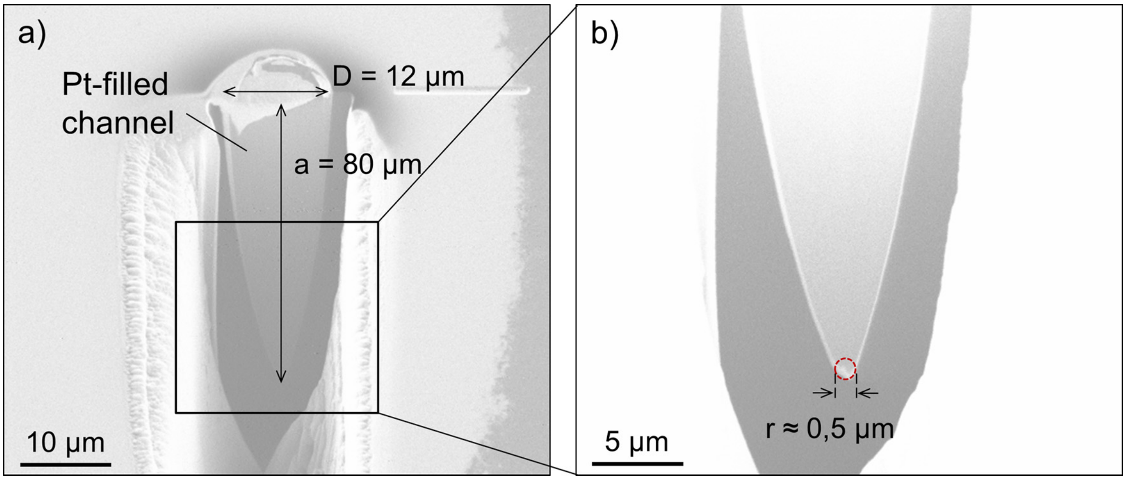

Fig. 7. FIB images of the cross section of a FIB-milled filament used for calibration. a) Image showing the whole filament, completely filled with platinum. b) Magnification of the filament tip showing a tip radius of approx. 0.5 µm.

prepared conductive filaments. The samples with sharpened root tips showed no difference in comparison to the not sharpened ones as can be seen in Table 3. It is clearly seen that the breakdown strength decreases with filament length. In samples with 50 µm filaments but reversed polarity at breakdown test the dielectric breakdown was not initiated at the conductive filament. There was no influence of the filaments perceptible and the samples behaved like sound ones.

As the dielectric breakdown initiated at the artificially introduced filaments ≥ 30 µm, all breakdown strength results from filaments between 30–100 µm length were fitted by a least square fit assuming the $\frac{1}{\sqrt{a}}$-dependence given in Eq. (3) and shown by the dotted grey line beyond a = 30 µm in Fig. 9. It can be seen that the experimentally measured dielectric breakdown strength fit well to the prediction. From the experimental results the calculated mean dielectric breakdown toughness G_{bd} applying Eqs. (1) and (2) is 6.30 ± 0.95 mJ/m using the geometrical and physical values given in Table 1.

4. Discussion

On the working hypothesis that dielectric breakdown is initiated by tiny electrically conducting filaments dielectric breakdown measurements with artificially introduced conducting filaments were conducted

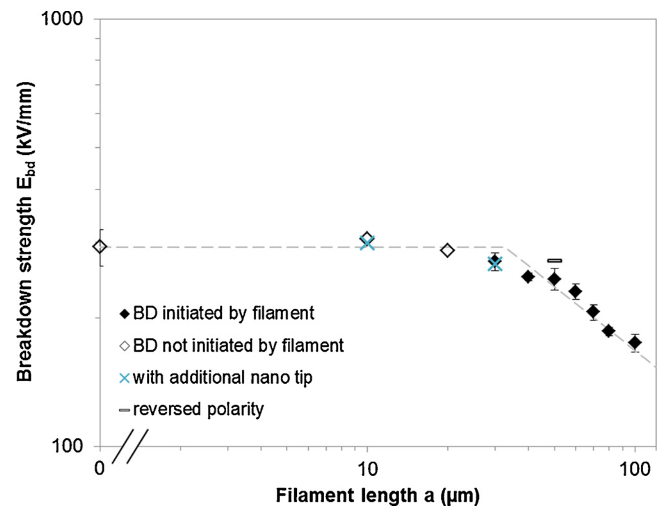

Fig. 9. Double logarithmic plot of the measured dielectric breakdown strength E versus filament length a.

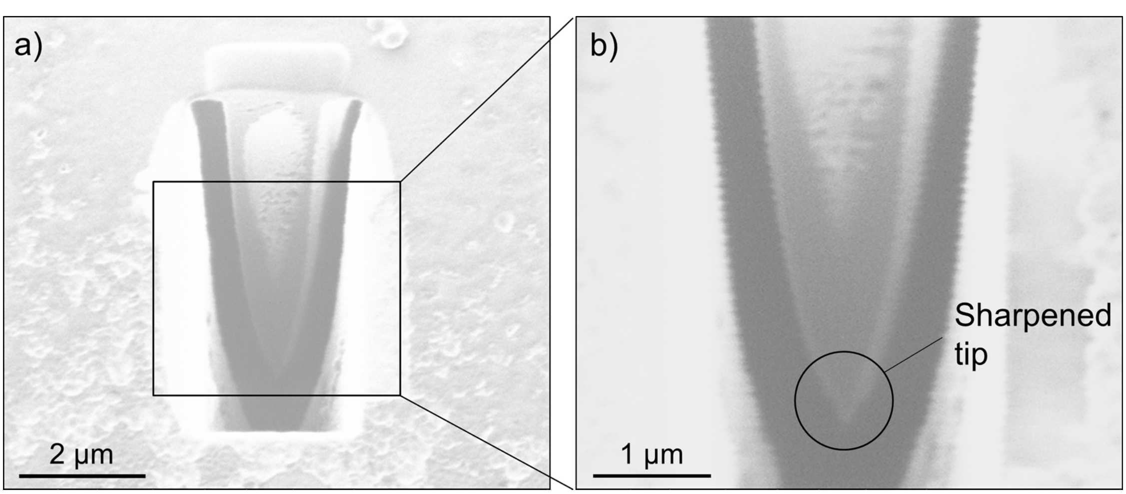

Fig. 8. FIB picture of a 10 µm filament with sharpened root tip. As this was a test filament, it was just roughly filled with Pt, which is seen at the bright region in the middle of the filament. Because the sharpened root tip is so small, it is difficult to picture it under a single beam FIB. While trying to focus the tiny tip under the ion beam the surrounding material got charged and additionally material was slowly removed and thereby the sharpened tip disappeared after a while. Therefore, we have no high quality image of the sharpened tip.

Table 3
Mean dielectric breakdown strength and standard deviation for all samples with different conductive filaments. For 10 µm and 30 µm it is also distinguished between a 500 nm and 50 nm root tip radius.

Filament length a [µm]	Root tip radius r [nm]	Breakdown strength E_{bd} [kV/mm]
10	500	275.0 ± 16.5
	50	299.5 ± 9.0
20	500	286.7 ± 0.0
30	500	270.9 ± 13.2
	50	266.9 ± 6.0
40	500	248.9 ± 5.2
50	500	245.9 ± 14.4
60	500	230.3 ± 10.0
70	500	206.1 ± 8.6
80	500	186.0 ± 4.2
100	500	174.7 ± 8.5

in 163 ± 7 µm thick borosilicate glass plates. The results showed that filament lengths of up to 30 µm did not change the dielectric breakdown strength of 292.87 ± 28.88 kV/mm of the sound glass. Filaments with lengths of 10 and 20 µm were not sufficient for the initiation of breakdown and the experimentally observed breakdown channels were detected at different locations underneath the negative electrode. Thus, it can be concluded that there is a kind of "natural" filament length of up to 20 µm existing in the sound glass. Only for filament lengths of 30 µm and longer the breakdown could be detected to initiate at the filament. Hence only these filament lengths where fitted by a $\frac{1}{\sqrt{a}}$ -dependence and showed very good agreement, as predicted by Eq. (3). From the known filament length and the obtained results for the breakdown strength, the dielectric breakdown toughness G_{bd} was calculated as 6.30 ± 0.95 mJ/m. We point out that Eq. (3) was developed for a spherical specimen with a conducting filament in its center. Therefore Eq. (3) is only an approximation for small conducting surface filaments in a plate as the Griffith solution for cracks is only an approximation for surface cracks. Nevertheless the experimental results reveal $\frac{1}{\sqrt{a}}$ -dependence up to 100 µm filament length and we used these data for the evaluation of the breakdown toughness. Further electrical breakdown analysis is necessary to validate this approach.

This determined breakdown toughness of 6.30 mJ/m is at the upper limit of estimations for Al_2O_3, TiO_2 and $BaTiO_3$ with 1.25 mJ/m, 2.21 mJ/m and 4.22 mJ/m, respectively, based on the transition thickness between extrinsic and intrinsic dielectric breakdown [5]. Lin et al. [21] determined a critical *J*-integral between 2–40 mJ/m for PZT (PZT807) in cylindrical specimen with 5–7 mm long initial channels and a channel radius of 0.3-0.7 mm. The *J*-integral evaluation is based on a perfect insulating dielectric material.

The Griffith type energy release rate model [1] assumes SCLC, which is found to be the dominant conduction mechanism in borosilicate glass before dielectric breakdown as shown in Fig. 5. At low voltages the slope of $s = 1$ of the data points indicates ohmic conduction in a double logarithmic *J*-*U*-diagram. Above a certain transition voltage U_{tr} SCLC is the dominating conduction mechanism, meaning that more charge carriers are injected into the sample through the electrode than thermal carriers are present. This phenomenon is characterized by a slope of ≥ 2 in the double logarithmic plot of Fig. 5. For a perfect insulator with shallow traps on one energy level the current density of SCLC J_{SCLC} is exactly [8]

$$J_{SCLC} = \frac{9}{8}\,\Theta\,\varepsilon_0\,\varepsilon_r\,\mu\,\frac{U^2}{d^3} \tag{4}$$

with the ratio of the free to the trapped carriers Θ (Θ = 1 for an ideal insulator without traps) and the charge carrier mobility µ. For a distribution of the energy levels of the traps, $J_{SCLC} \propto U^s$, where s can be more than 2. From the experimental date the transition from ohmic to SCL conduction occurs between 3 and 5 kV in this borosilicate glass. Thus, the conductivity measurements show a similar behavior as those on Al_2O_3 by Talbi et al. and Neusel et al. [14,11]. In these experiments it could be shown that Schottky and Poole-Frenkel conduction can be excluded as dominating conduction mechanism. The fact that breakdown tests with reversed polarity don't show breakdown initiation from the positively charged artificially introduced filament is an indication that electron injection is the source of the dielectric breakdown in the used borosilicate glass. These and previous findings support the notion that models, which are based on ohmic conduction, are not appropriate to describe the dielectric breakdown correctly.

In order to investigate whether the radius of curvature of the filament tip influences the dielectric breakdown strength for filaments with 10 and 30 µm length tip radii of 50 nm were FIBed. For the 10 µm long filaments, a sharper tip radius of 50 nm did not cause the breakdown to be initiated at the filament tip. For the 30 µm long filament, breakdown initiated at the filament tip but the dielectric breakdown strength did not change significantly in comparison to the 500 nm sized tip radii. As sharp edges and points tips are well known to increase the electric field strength, this result is astonishing. In a perfect dielectric the electric field E at the surface of a charged sphere of radius r scales with $E \propto \frac{1}{r^2}$ and a field enhancement of a factor of 100 is expected decreasing the filament tip radius from 500 to 50 nm. If SCLC prevails, the electric field at the surface of a conducting sphere is proportional to $E \propto \frac{1}{\sqrt{r}}$ [13], meaning that a 10 times smaller filament tip radius leads to a roughly 3 times higher field. The comparison of the 2 scenarios is in favour of a space charge mechanism in the sense that the local field strength at the filament tip is not decisive for breakdown but the electric energy released during filament extension.

5. Conclusion

The dielectric breakdown toughness for borosilicate glass was determined for the first time. The evaluation is based on SCLC as the dominant conduction mechanism right before breakdown. It was shown that FIB-milled filaments with lengths up to 20 µm do not initiate breakdown. Hence it is concluded that "natural" filaments of this size should exist underneath the electrodes. By changing the filament tip radius we could demonstrate that tip radii of 500 nm are small enough for a tip radii independent result. The FIB-milled channels are narrow and sharp enough to serve as model filaments and the extrinsic dielectric breakdown strength follows the $\frac{1}{\sqrt{a}}$ -dependence as predicted from a Griffith-type breakdown model. We assume that this experimental approach can be used to measure the breakdown toughness of other dielectric materials. Understanding the nature of these initial conducting filaments may enable to tailor the chemistry and microstructure of dielectric materials towards better breakdown resistance. In addition also further theoretical work is needed to determine the electrical breakdown energy release rate as function of the filament length for different sample geometries.

Acknowledgement

This work was supported by the German Research Foundation (DFG) under project number SCHN-372/17-2.

References

[1] G.A. Schneider, A griffith type energy release rate model for dielectric breakdown under space charge limited conductivity, J. Mech. Phys. Solids 61 (2013) 78–90, http://dx.doi.org/10.1016/j.jmps.2012.09.005.

[2] J.J. O'Dwyer, Dielectric breakdown in solids, Adv. Phys. 7 (27) (1958) 349–394, http://dx.doi.org/10.1080/00018735800101297.

[3] L.A. Dissado, J.C. Fothergill, Electrical Degradation and Breakdown in Polymers, P. Peregrinus, London, 1992.

[4] M. Nafria, J. Suñé, X. Aymerich, Breakdown of thin gate silicon dioxide films – a review, Microelectron. Reliab. 36 (7/8) (1996) 871–905, http://dx.doi.org/10.1016/0026-2714(96)00023-6.

[5] C. Neusel, G.A. Schneider, Size-dependence of the dielectric breakdown strength

from nano- to millimeter scale, J. Mech. Phys. Solids 63 (2014) 201–213, http://dx.doi.org/10.1016/j.jmps.2013.09.009.
[6] Y. Sun, S.A. Boggs, R. Ramprasad, The intrinsic electrical breakdown strength of insulators from first principles, Appl. Phys. Lett. 101 (2012) 132906, , http://dx.doi.org/10.1063/1.4755841.
[7] H.R. Zeller, W.R. Schneider, Electrofracture mechanics of dielectric aging, J. Appl. Phys. 56 (1984) 455, http://dx.doi.org/10.1063/1.333931.
[8] I.O. Owate, R. Freer, The Electrical Properties of Some Cordierite Glass Ceramics in the System MgO-Al2O3-SiO2-TiO2, (1990), http://dx.doi.org/10.1007/BF00580163.
[9] I.O. Owate, R. Freer, Ac breakdown characteristics of ceramic materials, J. Appl. Phys. 72 (1992) 2418–2422, http://dx.doi.org/10.1063/1.351586.
[10] Talbi, Lalam, Malec, Dielectric breakdown characteristics of Alumina, IEEE. (2010), http://dx.doi.org/10.1109/ICSD.2010.5568235.
[11] C. Neusel, H. Jelitto, G.A. Schneider, Electrical conduction mechanism in bulk ceramic insulators at high voltages until dielectric breakdown, J. Appl. Phys. 117 (2015) 154902, , http://dx.doi.org/10.1063/1.4917208.
[12] Hoshina, et al., Dielectric Breakdown Mechanism of Perovskite-Structured Ceramics, (2015), http://dx.doi.org/10.4071/CICMT-TP43.
[13] M.A. Lampert, P. Mark, Current Injection in Solids, Academic Press, New York, London, 1970.
[14] F. Talbi, F. Lalam, D. Malec, DC conduction of Al2O3 under high electric field, J. Phys. D: Appl. Phys. 40 (2007) 3803–3806, http://dx.doi.org/10.1088/0022-3727/40/12/037.
[15] R.L. Bertolotti, Fracture toughness of polycrystalline Al2O3, J. Am. Ceram. Soc. 56 (1973) 107, http://dx.doi.org/10.1111/j.1151-2916.1973.tb12373.x.
[16] D. Munz, T. Fett, Mechanisches Verhalten keramischer Werkstoffe: Versagensablauf, Werkstoffauswahl, Dimensionierung, Springer-Verlag, Berlin, 1989.
[17] T. Nishida, Y. Hanaki, G. Pezzotti, Effect of notch-root radius on the fracture of a fine-grained alumina, J. Am. Ceram. Soc. 77 (1994) 606–608, http://dx.doi.org/10.1111/j.1151-2916.1994.tb07038.x.
[18] C. Neusel, H. Jelitto, D. Schmidt, R. Janssen, F. Felten, G.A. Schneider, Dielectric breakdown in alumina single crystals, J. Eur. Ceram. Soc. 32 (2012) 1053–1057, http://dx.doi.org/10.1016/j.jeurceramsoc.2011.11.013.
[19]] Data sheet Th. Geyer, LabSolut, Borosilikatglas 3.3, 03/2013.
[20] R. Damani, R. Gstein, R. Danzer, Critical notch-root radius effect in SENB-S fracture toughness testing, J. Eur. Ceram. Soc. 16 (1995) 695–702, http://dx.doi.org/10.1016/0955-2219(95)00197-2.
[21] S. Lin, Dielectric Breakdown of an Unpoled Piezoelectric Material With a Conductive Channel, (2009), http://dx.doi.org/10.1111/j.1460-2695.2009.01362.x.